RSC Advances

PAPER

View Article Online
View Journal | View Issue

Cite this: RSC Adv., 2015, 5, 15861

Preparation of reduced graphene oxide/Cu nanoparticle composites through electrophoretic deposition: application for nonenzymatic glucose sensing†

Qian Wang,[ab] Qi Wang,[b] Musen Li,[b] Sabine Szunerits[a] and Rabah Boukherroub*[a]

Received 8th November 2014
Accepted 26th January 2015

DOI: 10.1039/c4ra14132f

www.rsc.org/advances

The paper reports on the simultaneous reduction/deposition of reduced graphene oxide/copper nanoparticles (rGO/Cu NPs) on a glass/Ti/Au electrode using an electrophoretic deposition (EPD) technique from a colloidal suspension of graphene oxide (GO) and copper sulphate ($CuSO_4$) in ethanol. The method allows controlling the nanoparticle density by adjusting the deposition time. Structural characterization and chemical composition analysis of the modified electrode showed the simultaneous reduction of GO with the concomitant deposition of metallic CuNPs with a $Cu(OH)_2$ shell. The electrocatalytic activity of the modified electrode was evaluated for non-enzymatic glucose sensing in alkaline medium. While the Au electrode modified only with rGO did not show obvious electrocatalytic activity, the electrode coated with rGO/CuNPs exhibited excellent electrocatalytic behavior towards glucose oxidation with a high sensitivity of 447.65 $\mu A\ mM^{-1}\ cm^{-2}$. The response current of the sensor is linear to glucose concentrations up to 1.2 mM with a detection limit of 3.4 μM. Furthermore, the interference from various oxidizable molecules such as dopamine, uric acid, ascorbic acid and carbohydrate molecules such as fructose, lactose and galactose was negligible, indicating a good selectivity of detection. The application of this glucose sensor in real samples has also been demonstrated successfully.

1. Introduction

The development of sensitive and selective methods for glucose detection is of significant importance not only for use in blood sugar monitoring, but also in the food industry, bio-processing, and in the development of renewable and sustainable fuel cells.[1] The great significance of glucose sensing has generated continuous efforts in the development of various detection schemes based on optical, fluorescence and electrochemical methods.[2–5]

Electrochemical glucose sensors generally fall into two categories *viz.* enzymatic and non-enzymatic.[1,3,6–8] Although enzymatic biosensors for glucose sensing display high sensitivity and selectivity, there are several drawbacks associated with enzyme-modified electrodes such as the high cost of enzymes, long-term stability and complexity of immobilization.[1] Furthermore, the enzyme activity can be easily affected by humidity, temperature and pH of the sensing medium.

Over the past decade, there has been an increasing interest in the development of non-enzymatic glucose sensors.[6–8] The preparation of a large variety of nanomaterials of different chemical nature and morphology has introduced a plethora of highly selective and sensitive glucose sensors.[6] Even though most of non-enzymatic glucose sensors are not selective towards other carbohydrates such as fructose and sucrose and need to be often operated in an alkaline medium, they have several advantages such as low cost, simplicity, reproducibility, fast response time, higher sensitivity and better stability than glucose oxidase-based interfaces. Copper-based electrodes represent an interesting class of materials for electrocatalytic oxidation of glucose. Indeed, carbohydrate oxidation at Cu electrode in alkaline media has been investigated in the early 90s.[9,10] It has been suggested that Cu(III) was involved in the electrocatalytic oxidation process of the carbohydrates. Emergence of nanotechnological tools allowed the synthesis of Cu-based nanomaterials of different shapes and morphologies and their application for non-enzymatic glucose sensing.[11–15]

Recently, graphene has captured great interest among physicists, chemists, and materials scientists and has brought significant progress to applied electrochemical fields.[16–18] In

---

[a] *Institut de Recherche Interdisciplinaire (IRI, USR CNRS 3078), Université Lille 1, Parc de la Haute Borne, 50 Avenue de Halley, BP 70478, 59658 Villeneuve d'Ascq, France. E-mail: rabah.boukherroub@univ-lille1.fr; Fax: +33 362 53 17 01; Tel: +33 362 53 17 24*

[b] *Key Laboratory for Liquid–Solid Structural Evolution and Processing of Materials, Shandong University, Jinan 250061, China*

† Electronic supplementary information (ESI) available. See DOI: 10.1039/c4ra14132f

fact, graphene displays outstanding properties such as high surface area, good electrical conductivity, mechanical flexibility and chemical stability. Furthermore, chemically derived graphene (and its derivatives) exhibits a high density of edge-plane-like defect sites, which might provide many active sites for electron transfer to chemical and biological species.[19] These properties have made graphene an effective biosensing interface of different biomolecules and biologically relevant molecules such as H_2O_2, glucose, dopamine, ascorbic acid, uric acid, protein, DNA, cholesterol, histidine, organosulfate pesticides, nicotinamide adenine dinucleotide (NADH), *etc.*[19,20] Another important aspect is the ease of graphene functionalization through covalent or non covalent pathways and its use as a 2D support for loading various polymers or nanoparticles, giving rise to nanohybrid materials with original properties. The resulting functional nanomaterials and nanocomposites display improved performance due to synergistic effects interaction.

In the last few years, the preparation of Cu-based nanostructures/graphene composites represents a burgeoning field of research for various applications such as electrodes in electrochemical supercapacitors,[21] electrochemical sensing platform for simultaneous determination of dopamine and ascorbic acid,[22] surface-enhanced Raman scattering (SERS) active substrate,[23] hydrolytic dehydrogenation of ammonia borane,[24] and catalysis.[25,26] Copper nanostructures/graphene nanocomposites have also been investigated for non enzymatic glucose sensing.[27–33] The sensors showed detection limits ranging from 80 nM to 1.3 μM, depending on the preparation conditions and composition of the nanocomposite, the deposition mode, the supporting electrode material, and the electrochemical technique employed. Different strategies have been used for the preparation of the Cu nanostructures/graphene composites. They consist on the direct electrochemical reduction of Cu salt on GC electrode previously coated with reduced graphene oxide (rGO),[28,29,32] and *in situ* reduction of GO–Cu salt using potassium borohydride,[27] sodium borohydride,[31] and glycine at 500 °C.[30]

Electrophoretic deposition (EPD) is a well developed and cost-effective technique having a number of advantages such as high deposition rate, thickness controllability, good uniformity and simplicity of scale up for the preparation of thin films from charged colloidal suspensions. In a recent report, we have shown that electrophoretic deposition (EPD) can be applied for the preparation of $Ni(OH)_2$ nanostructures modified rGO matrices in a reproducible manner and successfully used the resulting Ni–graphene nanocomposite for non-enzymatic determination of glucose with a detection limit of 15 μM.[34] Here, we report on the fabrication of non-enzymatic sensor based on copper nanoparticles (Cu NPs)/rGO nanocomposite. The nanocomposite was prepared using EPD technique, consisting on simultaneous deposition/reduction of Cu NPs/rGO from an ethanolic solution of GO and Cu salt. The nanocomposite showed a good electrocatalytic activity toward glucose oxidation with a good sensitivity and detection limit.

2. Experimental

2.1. Materials

All chemicals were reagent grade or higher and were used as received unless otherwise specified. Graphite powder (<20 micron), potassium permanganate ($KMnO_4$), sulphuric acid (H_2SO_4), phosphoric acid (H_3PO_4), hydrogen peroxide (H_2O_2), copper sulphate ($CuSO_4$), sodium hydroxide (NaOH), glucose, uric acid (UA), ascorbic acid (AA), dopamine hydrochloride (DA), fructose, lactose, galactose, phenol, and ethanol were purchased from Sigma-Aldrich. The water used throughout the experiments was purified with a Milli-Q system from Millipore Co. (resistivity = 18 MΩ cm).

2.2. Preparation of graphene oxide (GO)

GO nanosheets were produced from natural graphite powder by an improved Hummers and Offeman method. The detailed experimental conditions are reported in a recently published work.[35] A homogeneous yellow brown suspension (0.5 mg mL^{-1}) of GO sheets in water was achieved by ultrasonication for 3 h.

2.3. Preparation of rGO modified gold interfaces by electrophoretic deposition

Gold electrodes were prepared by vacuum deposition of 5 nm of titanium and 48 nm of gold onto cleaned glass slides (76 × 26 × 1 mm^3, $n = 1.58$ at $\lambda = 633$ nm, CML, France). The electrophoretic deposition (EPD) was carried out using a two-electrode cell containing the GO aqueous dispersion (0.5 mg mL^{-1}) by applying a DC voltage (50 V) for 2 min. Platinum (Pt) foil (1 × 2 cm^2) acts as the cathode and the gold substrate as the anode. The two electrodes are separated by 1 cm and are placed parallel to each other in the GO dispersion. After deposition, the interface was washed with deionized water (three times) followed by blow drying with nitrogen.

2.4. Preparation of rGO/Cu NPs-modified gold interfaces by electrophoretic deposition

The EPD was carried out in a two-electrode cell, where the two electrodes are placed parallel to each other and are separated by a distance of 1 cm. A platinum foil (1 × 2 cm^2) acts as the anode and the gold substrate as the cathode. GO/$CuSO_4$ suspensions were ultrasonicated for 30 min before use. The electrophoretic cell was then filled with a solution of GO (0.5 mg mL^{-1})/$CuSO_4$ (0.5 mg mL^{-1}) in ethanol and a DC voltage of 50 V was applied for 2 min. After deposition, the interfaces were rinsed with deionized water (three times) followed by blow drying with nitrogen. The modified electrodes were activated by cycling 15 times between −1 to and +0.2 V in NaOH (0.1 M) at a scan rate of 50 mV s^{-1}.

2.5. Preparation of CuNPs modified gold interfaces by electrophoretic deposition

The EPD was carried out using a two-electrode cell containing the $CuSO_4$ ethanolic dispersion (0.5 mg mL^{-1}) by applying a DC voltage (50 V) for 2 min. Platinum (Pt) foil (1 × 2 cm^2) acts as the anode and the gold substrate as the cathode. The two electrodes are separated by 1 cm and are placed parallel to each other in the $CuSO_4$ dispersion. After deposition, the interface was washed with deionized water (three times) followed by blow drying with nitrogen. The modified electrodes were activated by cycling 15 times between −1 to and +0.2 V in NaOH (0.1 M) at a scan rate of 50 mV s^{-1}.

2.6. Determination of glucose content in human serum (colorimetric method)

A standard calibration curve for glucose was generated by mixing aliquots of aqueous phenolic solution (5 wt%, 1 mL) and concentrated H_2SO_4 (5 mL) to a series of 1 mL aqueous glucose solution (20, 40, 60, 80, 100 μg mL^{-1}). After shaking continuously for 10 min, the absorption spectrum (450–550 nm) was recorded using a phenol–H_2SO_4–water mixture as a blank. The absorbance ($\lambda_{max} \approx 490$ nm) difference was plotted against the glucose concentration. 50 μL of the human serum were diluted to 250 μL in water and mixed with 250 μL phenol/1.25 mL H_2SO_4 for glucose determination.[36,37]

2.7. Sample characterization

2.7.1. Scanning electron microscopy (SEM). Scanning electron microscopy images and energy dispersive X-ray (EDX) spectra of the films were obtained using an FEI Nova NanoSEM 450 scanning electron microscope with FEG (field emission gun, Schottky type) system equipped with an energy dispersive X-ray analyzer at an accelerating voltage of 20 kV.

2.7.2. X-Ray diffraction (XRD). The X-ray diffraction (XRD) patterns were recorded in the range of 10–90° on a Rigaku D/Max-kA X-ray diffractometer using Cu Kα radiation (λ = 1.54 Å) at 40 kV and 30 mA.

2.7.3. X-Ray photoelectron spectroscopy (XPS). XPS measurements were performed with an ESCALAB 220 XL spectrometer from Vacuum Generators featuring a monochromatic Al Kα X-ray source (1486.6 eV) and a spherical energy analyzer operated in the CAE (constant analyzer energy) mode (CAE = 100 eV for survey spectra and CAE = 40 eV for high-resolution spectra), using the electromagnetic lens mode. The detection angle of the photoelectrons is 30°, as referenced to the sample surface. The Au_{4f} at 84 eV was used to calibrate the other elements. After subtraction of the Shirley-type background, the core-level spectra were decomposed into their components with mixed Gaussian–Lorentzian (30 : 70) shape lines using the CasaXPS software. Quantification calculations were performed using sensitivity factors supplied by PHI.

2.7.4. Zeta potential measurements. The zeta potential of GO and GO/$CuSO_4$ (20 μg mL^{-1} in ethanol) was measured using the electrophoretic mode with the Zetasizer® Nano ZS (Malvern Instruments S.A., Worcestershire, UK).

2.7.5. Electrochemical measurements. Electrochemical experiments were performed using an Autolab potentiostat 20 (Eco Chemie, Utrecht, The Netherlands). Ag/AgCl (Bioanalytical Systems, Inc.) electrode was used as reference electrode, and platinum wire as counter electrode. The rGO/CuNPs–glass/Ti/Au electrode working electrode (A = 0.28 cm^2) was sealed against the bottom of a single compartment electrochemical cell by means of a rubber O-ring. The electrical contact was made to a copper plate, through the gold film onto which the rGO/CuNPs film was deposited. Cyclic voltammetry (CV) measurements were performed in aqueous solutions of 0.1 M NaOH in the absence and presence of glucose on rGO or rGO/CuNPs modified glass/Ti/Au electrodes.

Chronoamperometric detection of glucose on the glass/Ti/Au/GO–Cu NPs electrode was performed under N_2-saturated steady-state conditions in stirring alkaline solution (0.1 M NaOH) by applying a constant potential of +0.55 V to the working electrode. When the background current became stable (after 100 s), a subsequent addition of glucose was realized and the current was measured.

3. Results and discussion

Electrophoretic deposition (EPD) is a common industrial technique and cost effective method for the deposition of thin films from charged colloidal suspensions. In the recent years, it has been successfully applied for thin film deposition of graphene and carbon nanotubes,[38,39] and for the preparation of graphene-based nanocomposites.[40,41] We have successfully applied the EPD technique for coating glass/Ti/Au sensor with rGO for SPR sensing[42,43] or with rGO/$Ni(OH)_2$ for non-enzymatic glucose sensing.[34] In the present work, EPD was used for the deposition of rGO/Cu NPs from a colloidal solution of GO and $CuSO_4$ at 50 V on glass/Ti/Au electrode for different times (Fig. 1). GO produced by the Hummers method displays oxygen-based functional groups such as hydroxyl and epoxide on the basal planes, and carboxylate and carbonyl groups at the edges. The presence of these functional groups confers a negative charge to the material ($\zeta = -23 \pm 2$ mV). Addition of an equivalent amount of $CuSO_4$ resulted in a colloidal suspension with an overall positive zeta-potential ($\zeta = +15 \pm 2$ mV), making cathodic rather than anodic EPD feasible.

The morphology and chemical composition of rGO and rGO/CuNPs nanocomposite were characterized by scanning electron microscopy (SEM) and energy dispersive X-ray (EDX) analysis. Fig. 2a displays an SEM image of rGO deposited on Au/Ti/glass substrate from an aqueous solution of GO (0.5 mg mL^{-1}) at an applied voltage of 50 V for 2 min. It consists of a smooth and homogeneous film. EDX analysis performed on rGO modified Au/Ti/glass substrate shows signals due mainly to C, O, Ti, Au and Si (Table 1). This is in accordance with the chemical composition of the film and the underlying substrate. It should be noted that the EDX spectrum comprises signals due to Na, Mg and Ca impurities in the glass substrate with an overall atomic concentration of 12% (Fig. S1†). Characteristic SEM images of rGO/CuNPs nanocomposite obtained by EPD from an ethanolic solution of GO (0.5 mg mL^{-1}) and $CuSO_4$ (0.5 mg mL^{-1}) at an applied voltage of 50 V and a deposition time of 2 min are depicted in Fig. 2b and c. The presence of a homogeneous film of Cu NPs is clearly visible on Fig. 2b. The Cu NPs are 50 ± 7 nm average diameter (estimation from 200 nanoparticles). EDX analysis of the rGO/CuNPs film deposited on Au/Ti/glass substrate exhibits signals due to Cu, C,

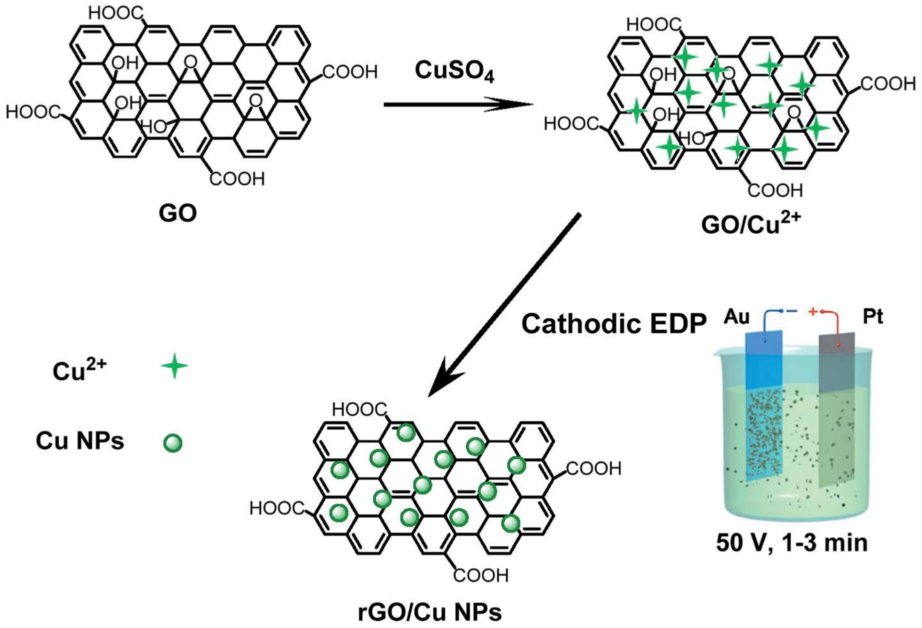

Fig. 1 Schematic illustration of the preparation of rGO/CuNPs using electrophoretic deposition/reduction.

O, Au and Si. The results are in good agreement with simultaneous Cu and rGO on the Au/Ti/glass substrate. The Cu atomic concentration was estimated to be 11.96 at% (Table 1). Signals due to Na and Mg and Ca (overall atomic concentration of 7.9%) are also present in the EDX spectrum of the rGO/CuNPs nanocomposite film (Fig. S2†).

We have investigated the influence of the deposition time on the morphology and sensing performance of the rGO/CuNPs film. SEM images of the nanocomposites deposited under otherwise similar experimental conditions [GO (0.5 mg mL^{-1}), $CuSO_4$ (0.5 mg mL^{-1}), $V = 50$ V] for 1 and 3 min are displayed in Fig. S3 and S5.† Compared to the sample prepared by EPD for 2 min, SEM images of the rGO/CuNPs film obtained after 1 min deposition show a comparable morphology, but a slightly lower density of CuNPs (Fig. S3†). The nanoparticles are 67 ± 6 nm in diameter (averaged over 200 nanoparticles). The EDX spectrum of the sample displays signals due to Cu, C, O, Au and Si with Cu atomic concentration of 5.72 at%, lower than that of the rGO/CuNPs film deposited for 2 min (Fig. S4†). In contrast, longer EPD time of 3 min gave a rGO/CuNPs film with much higher density of CuNPs (Fig. S5†) and increased Cu atomic concentration (16.35 at%) (Fig. S6†). The results are somehow different from the porous structures obtained in our previous study on $rGO/Ni(OH)_2$ thin films deposited using EPD on Au interfaces.[34]

The crystalline phase of the as-prepared substrates was characterized by X-ray diffraction (XRD) in the range of 10–90°. Fig. 3 illustrates the XRD patterns of rGO and rGO/CuNPs deposited through EPD. The XRD pattern of rGO deposited on glass/Ti/Au sensor displays a broad peak at 24.2° and a small peak at 44.3° (corresponding to the indices of (002) and (100)) characteristic of graphene, and peaks of the underlying Au substrate at 38.3° and 81.6° corresponding to (111) and (222) crystalline planes, respectively (Fig. 3a). The XRD patterns of rGO/CuNPs deposited by EPD from an ethanolic solution of GO (0.5 mg mL^{-1}) and $CuSO_4$ (0.5 mg mL^{-1}) at an applied voltage of 50 V for 1–3 min are depicted in Fig. 3b–d. An additional peak at 2θ value of 43.3° corresponding to Cu(111) crystalline plane appears, in accordance with Cu deposition.

X-Ray photoelectron spectroscopy (XPS) analysis results also confirmed the formation of rGO/CuNPs nanocomposite. The C1s core level XPS spectrum of GO nanosheets is displayed in Fig. S7.† It can be deconvoluted into four components with binding energies at about 283.8, 284.7, 286.7 and 287.9 eV assigned to sp^2-hybridized carbon, C–H/C–C, C–O and C=O species, respectively. The spectrum is dominated by the peak at 286.7 eV due to C–O, in accordance with a high oxidation degree of GO. Fig. 4a depicts the high resolution XPS C1s core level spectrum of the glass/Ti/Au electrode interface modified with rGO/CuNPs. It can be deconvoluted into three peaks at 284.08 eV (Csp^2), 285.1 eV (Csp^3) and 287.80 eV (C=O) with the Csp^2 component being dominant, suggesting GO reduction during EPD deposition. The high resolution of the core level of Cu 2p reveals the presence of several peaks with binding energies at 932.66, 934.2, 941.83, 951.46, 953.94, and 960 eV. The peaks at 932.66 and 951.46 eV are attributed to Cu $2p_{3/2}$ and Cu $2p_{1/2}$, respectively from metallic Cu^0 or Cu^+ (Cu_2O). Unfortunately, Cu^0 cannot be distinguished from Cu^+ by XPS because of their spectral overlap.[44,45] However, based on the literature data, the peak is most likely due to Cu^0 (the ISO standard Cu metal line is at 932.63 eV with a deviation set at ±0.025 eV).[45] The peaks at 934.2 and 953.94 eV are due to Cu $2p_{3/2}$ and Cu $2p_{1/2}$, respectively from Cu^{2+}. These peaks arise from $Cu(OH)_2$ rather than CuO.[15,45] In addition, the presence of shake-up satellite peaks at higher binding energies *i.e.* 941.83 and 960 eV, characteristic of materials having a d^9 configuration in their ground state, clearly indicates the presence of Cu^{2+}. The overall Cu content is 10.4 at%, indicating high loading of Cu NPs onto the rGO surface. The result is consistent with EDX analysis (11.96%)

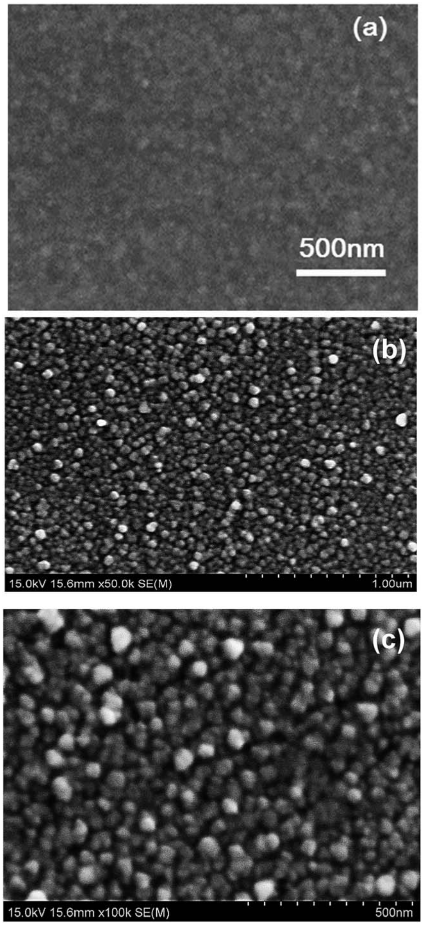

Fig. 2 Scanning electron microscopy (SEM) images of rGO and rGO/CuNPs deposited by EPD technique using an ethanolic solution of GO (0.5 mg mL^{-1}) and GO (0.5 mg mL^{-1}) + $CuSO_4$ (0.5 mg mL^{-1}), respectively. Applied voltage: 50 V; deposition time = 2 min.

Table 1 EDX results of rGO and rGO/CuNPs deposited by EPD technique using GO and GO + $CuSO_4$ in ethanol, respectively. Applied voltage: 50 V, deposition time = 2 min; GO (0.5 mg mL^{-1}), $CuSO_4$ (0.5 mg mL^{-1})

Element	rGO (at%)	rGO/CuNPs (at%)
Cu K	—	11.96
C K	19.76	21.40
O K	26.20	24.21
Ti K	0.80	—
Au M	10.30	9.68
Si K	30.98	24.85

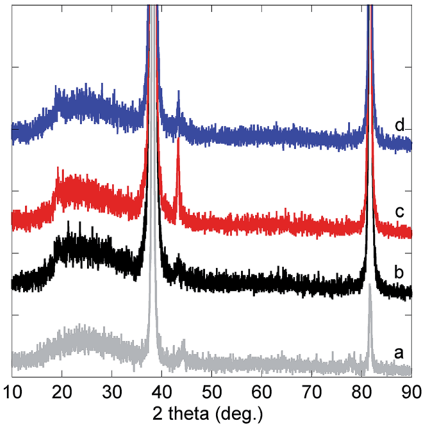

Fig. 3 X-Ray diffraction patterns of rGO (a) and rGO–Cu NPs deposited by EPD technique using 0.5 mg mL^{-1} of GO and 0.5 mg mL^{-1} of $CuSO_4$ in ethanol for 1 min (b), 2 min (c) and 3 min (d). Applied voltage: 50 V; deposition time = 1–3 min.

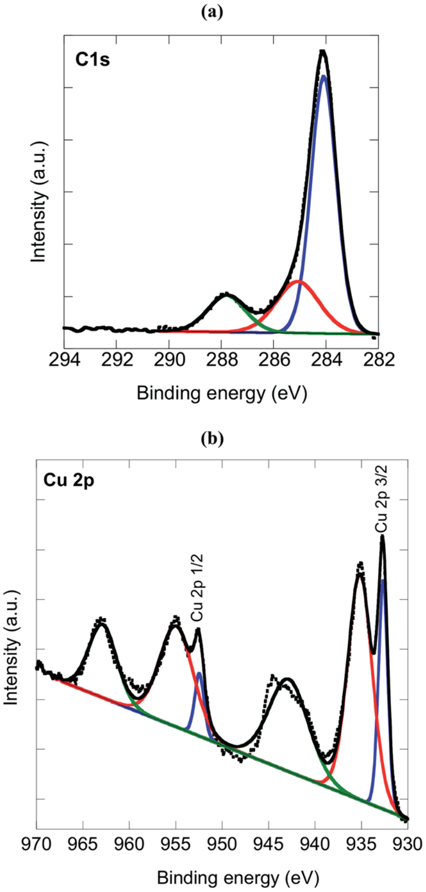

Fig. 4 High resolution X-ray photoelectron spectroscopy (XPS) (A) C1s and (B) Cu 2p core level spectra of rGO/CuNPs modified glass/Ti/Au electrode deposited by EPD (50 V, 2 min).

of the same sample (Table 1). However, this value is slightly lower than 15.9 at% determined for Ni upon EPD of rGO/$Ni(OH)_2$ under otherwise similar experimental conditions.[34]

The electrochemical behavior of the rGO/CuNPs in N_2-staturated 0.1 M NaOH aqueous solution was evaluated by cyclic voltammetry (CV). Before investigating the electrocatalytic performance of the nanocomposite material toward glucose oxidation, the rGO/CuNPs modified Au/Ti/glass electrode was cycled between −1 V to +0.2 V in 0.1 M NaOH till a steady-state *j*–*E* was obtained (Fig. 5). The anodic peaks at −0.35 V and −0.12 V correspond to the transitions Cu^0/Cu(I) and Cu(I)/Cu(II), respectively. In the cathodic scan, the peaks at −0.38 V and −0.80 V correspond to the re-formation of Cu(I) and Cu^0,

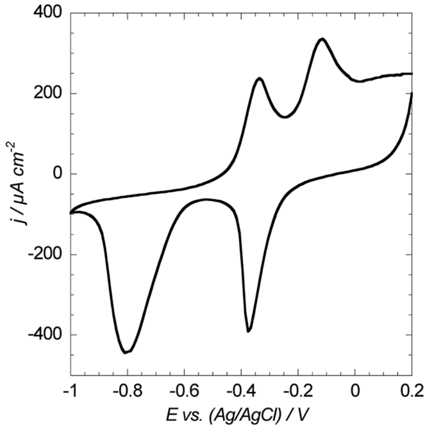

Fig. 5 Cyclic voltammograms of rGO/CuNPs deposited by EPD (50 V, 2 min) on glass/Ti/Au electrode in N_2-saturated 0.1 M NaOH aqueous solution (potential between −1 V and +0.2 V), scan rate: 50 mV s^{-1}.

respectively. This behavior is similar to those reported for copper and copper nanowire electrodes in NaOH aqueous solution.[9,10,14]

In order to investigate the applicability of the rGO/CuNPs modified Au/Ti/glass electrode for non-enzymatic glucose sensing, a simplified analysis was carried out in the potential range from +0.2 V to +0.8 V, which is more pertinent for amperometric detection of glucose. Fig. 6 depicts the CVs of the rGO/CuNPs (deposition time = 2 min) modified Au/Ti/glass electrode in N_2-saturated 0.1 M NaOH aqueous solution in the absence and presence of 1 mM glucose. A significant increase of the anodic current is obvious upon addition of glucose, suggesting a good electrocatalytic activity of the rGO/CuNPs film toward glucose oxidation. In contrast, only a slight anodic current increase at the potential above +0.5 V can be detected in the presence of glucose on rGO modified Au/Ti/glass electrode, indicating that rGO alone deposited by EPD under our experimental conditions (EPD deposition from 0.5 mg mL^{-1} of GO in ethanol at 50 V for 2 min) is not electroactive toward glucose oxidation (data not shown). Furthermore, we tested the electrocatalytic activity of CuNPs modified Au/Ti/glass electrode toward glucose oxidation (Fig. S8†). The electrode was prepared by EPD from 0.5 mg mL^{-1} of $CuSO_4$ in ethanol (applied voltage: 50 V; deposition time = 2 min). Although the electrode showed an increase of the anodic current upon addition of 1 mM glucose in N_2-saturated 0.1 M NaOH aqueous solution, the anodic current remains lower than that recorded on rGO/CuNPs modified Au/Ti/glass electrode. The results clearly suggest a synergistic effect of rGO and CuNPs in the electrocatalytic system. Similarly, the CVs of rGO/CuNPs modified Au/Ti/glass electrodes (deposition times = 1 and 3 min) were recorded in the presence of 1 mM glucose in the potential range of 0.2–0.8 V under otherwise identical conditions. Both samples showed lower currents compared to the electrode prepared through EPD deposition for 2 min. This sample was then investigated throughout this work.

The electrocatalytic response of Au/Ti/glass electrode modified with rGO/CuNPs to glucose was further investigated by amperometric current–time response upon successive addition of different concentrations of glucose. Fig. 7a displays the amperometric response of the modified electrode at an applied potential of +0.55 V *vs.* Ag/AgCl. The oxidation current increased

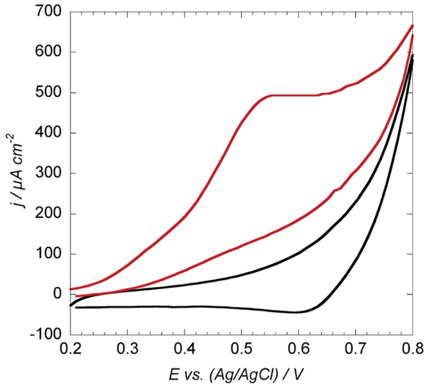

Fig. 6 Cyclic voltammograms of rGO/CuNPs deposited by EPD (50 V, 2 min) on glass/Ti/Au electrode in N_2-saturated 0.1 M NaOH aqueous solution in the absence (black) and presence (red) of 1 mM glucose, scan rate: 50 mV s^{-1}.

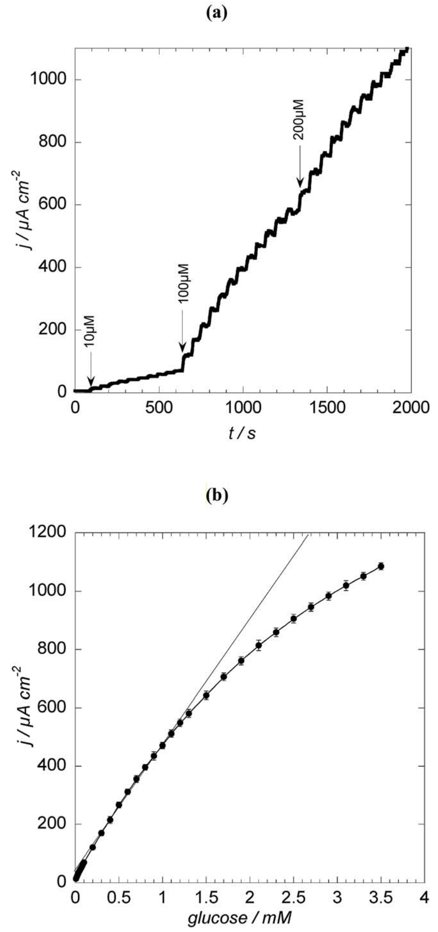

Fig. 7 (A) Amperometric response of rGO/CuNPs modified glass/Ti/Au electrode polarized at +0.55 V *vs.* Ag/AgCl in N_2-saturated 0.1 M NaOH aqueous solution with subsequent addition of glucose (10 μM, 100 μM or 200 μM); (B) the corresponding calibration curve.

Table 2 Comparison of analytical performance of other Cu/rGO-based non-enzymatic glucose sensors

Electrode	Detection limit (μM)	Sensitivity (μA mM^{-1} cm^{-2})	Linear range	Ref.
Cu_2O/SMWNTs[a]	0.2	2143	0.5 μM–2.5 mM	44
Cu@TiC/C nanofiber arrays	0.2	415	1 μM–1.7 mM	13
Cu–N-G[b]	1.3	48.13	0.004–4.5 mM	30
CuO–G–GCE[c]	0.7	1360	2 μM to 4 mM	29
Cu–graphene	0.5	—	Up to 4.5 mM	28
CuNPs–graphene	0.2	607	5 μM to 1.4 mM	32
CuNPs/PAA/GR[d]	0.08	—	0.3 μM–0.6 mM	31
CuNPS/MWCNTs[e]	0.5	50.47	10 μM–0.3 mM	47
Cu–CNTs[f]	0.21	17.76	0.7 μM–3.5 mM	48
Cu_2O–MWCNT	0.05	6.53	Up to 10 μM	49
CuO/MWCNTs	0.2	2596	0.4 μM–1.2 mM	50
CuOs-aSWCNT[g]	0.02	16.2	117–800 μM	51
Cu-MCE[h]	1.2×10^{-6}	—	62 μM–0.5 mM	52
CuCo-CFs/Nafion/GCE[i]	1.0	507	0.02–11 mM	53
CuNPs/rGO	3.4	447.65	0.01–1.2 mM	This work

[a] SMWNTs: straight multi-walled carbon nanotubes. [b] Cu–N-G: copper nanoparticles decorated nitrogen-doped graphene. [c] CuO–G: copper oxide (CuO) nanocubes–graphene. [d] CuNPs/PAA/GR: copper nanoparticles/polyacrylic acid/graphene. [e] MWCNTs: multiwalled carbon nanotubes. [f] Cu–CNTs: copper nanoclusters–multiwall carbon nanotubes. [g] COs-aSWCNT: copper oxide nanoparticles on horizontally aligned single-walled carbon nanotube arrays. [h] Cu-MCE: Cu-based chemically modified electrode (CME). [i] CuCo-CFs: Bimetallic CuCo nanoparticles doped-carbon nanofibers.

gradually upon injection of increasing concentrations of glucose into the NaOH solution and reached the maximum steady state current within 15 s. Fig. 7b shows the corresponding calibration curve of the current response *versus* glucose concentration. A linear current-response relationship was obtained as a function of glucose concentration from 0.01 to 1.2 mM with j (μA mM^{-1} cm^{-2}) = 24.892 + 447.65 [glucose], $R = 0.998$ with an estimated sensitivity of 447.65 μA mM^{-1} cm^{-2}. A detection limit of 3.4 μM at a signal-to-noise ratio of 3 was achieved using glass/Ti/Au electrode modified with rGO/CuNPs. The detection limit determined for the sensor is higher than 0.08 to 1.3 μM reported in the literature for copper-based/rGO or carbon nanotube electrodes prepared using various approaches (Table 2).[13,28–32,46–53] However, the proposed strategy for the preparation of metal oxide nanoparticles/rGO is a one-pot, straightforward, and environmentally friendly approach that can be easily used for the integration of other nanoparticles on the same matrix and thus opens up new routes in the design of more sensitive sensors.

The detection of glucose is often hampered by the presence of oxidizable molecules, which can compromise the selectivity of detection and hence the overall accuracy of measurement.[6] To evaluate the selectivity of the nanocomposite, a number of oxidizable and interfering molecules such as dopamine (DA), ascorbic acid (AA), uric acid (UA) and other carbohydrate derivatives such as fructose, lactose and galactose were examined at the glass/Ti/Au electrode modified with rGO/Cu NPs. Fig. 8 compares the amperometric response of the glass/Ti/Au electrode coated with rGO/CuNPs upon successive additions of glucose (500 μM), uric acid (UA, 50 μM), ascorbic acid (AA, 50 μM), dopamine (DA, 50 μM), fructose (50 μM), lactose (50 μM) and galactose (50 μM) in N_2-saturated 0.1 M NaOH aqueous solution at an applied potential of +0.55 V *vs.* Ag/AgCl. No significant current increase was detected upon addition of AA, UA and DA, as compared to amperometric response obtained upon glucose addition, suggesting that these species do not interfere with glucose detection under our experimental conditions. Similarly, no obvious response of the Au electrode coated with rGO/CuNPs was recorded upon addition of different interfering carbohydrate molecules at the physiological concentration level. The results indicate that the Au electrode modified with rGO/CuNPs exhibits a good selectivity toward glucose detection.

The practical applicability of the glass/Ti/Au electrode modified with rGO/Cu NPs for the determination of glucose concentration was tested in human serum samples. Fig. 9 exhibits the amperometric response of the glass/Ti/Au electrode coated with rGO/CuNPs upon successive additions of different analytes (standard glucose, human serum sample, AA and UA) in N_2-saturated 0.1 M NaOH aqueous solution at an applied potential of +0.55 V *vs.* Ag/AgCl. The concentration of glucose in

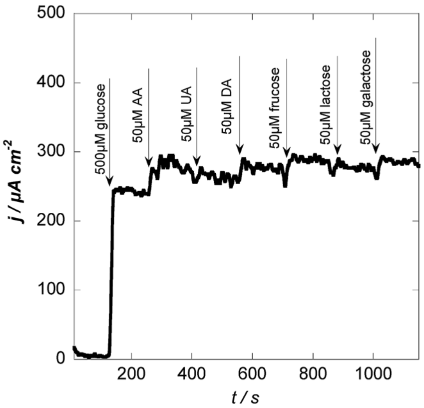

Fig. 8 The amperometric response of the rGO/CuNPs modified glass/Ti/Au electrode exposed to glucose (500 μM), ascorbic acid (AA), uric acid (UA), dopamine (DA), fructose, lactose and galactose (50 μM). Electrolyte: N_2-saturated 0.1 M NaOH aqueous solution. Potential: +0.55 V.

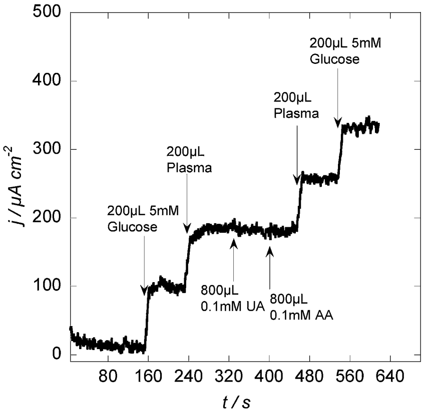

Fig. 9 The amperometric response of the rGO/CuNPs modified glass/Ti/Au electrode upon successive additions of different analytes. Electrolyte: N_2-saturated 0.1 M NaOH aqueous solution. Potential: +0.55 V.

the human serum sample was determined to be 4.7 mM by using the calibration curve in Fig. 7b. This glucose concentration is comparable to the concentration of 4.51 mM determined using the well-established phenol–sulphuric acid colorimetric method for the analysis of carbohydrates (Fig. S9†),[36,37] underlining the interest of the analytical approach described herein. Furthermore, the addition of 0.1 mM UA and 0.1 mM AA cause insignificant current increase, suggesting that these species do not interfere with glucose detection in real samples.

Finally, the repeatability of the Au electrode coated with rGO/CuNPs film was examined by measuring the current signal for 0.1 mM glucose at 6 modified electrodes produced under otherwise similar experimental conditions. A relative standard deviation (RSD) of 6.67% was determined, indicating good repeatability and reliability of the fabrication method. The long-term stability of the electrode was estimated after storage in a refrigerator at 4 °C for 2 weeks. The sensor retained about 89.6% of its initial current response to 0.1 mM glucose in 0.1 M NaOH aqueous solution at +0.55 V, suggesting a good stability of the electrode.

In conclusion, we have demonstrated that electrophoretic deposition can be easily applied for simultaneous reduction/deposition of thin films of rGO/CuNPs from an ethanol solution of GO and $CuSO_4$. The morphological and structural characterizations of the resulting nanocomposite revealed the reduction of GO accompanied by CuNPs deposition. Electrochemical measurements of Au electrode coated with rGO/CuNPs showed the characteristic redox peaks of a copper electrode behavior in alkaline media. The electrocatalytic activity of the resulting sensor was examined for non-enzymatic glucose oxidation in N_2-saturated 0.1 M NaOH aqueous solution. The electrochemical results showed that the sensor had a high sensitivity of 447.65 $\mu A\ mM^{-1}\ cm^{-2}$ with a detection limit of 3.4 μM over a linear range from 0.01 to 1.2 mM. Moreover, the sensor exhibited good selectivity for glucose oxidation in the presence of various oxidizable interfering species such as uric acid, ascorbic acid, dopamine and carbohydrate molecules such as fructose, lactose and galactose at physiological level. Moreover, the sensor has been successfully applied for the determination of glucose concentration in human blood serum samples. The excellent performance of the sensor combined with the good stability and reproducibility together with the ease of its fabrication make this technique very attractive for the preparation of sensing platforms of different electrochemical species. Finally, the good catalytic properties of CuNPs combined with the outstanding physico-chemical properties of rGO may find potential applications in various chemical transformations by taking advantage of the synergistic effects of rGO and CuNPs.

Acknowledgements

R.B. and S.S. gratefully acknowledge financial support from the Centre National de Recherche Scientifique (CNRS), the University Lille 1 and Nord Pas de Calais region. S.S thanks the Institut Universitaire de France (IUF) for financial support. Qian Wang thanks Chinese government for the China Scholarship Council Award. Qi Wang thanks "the Fundamental Research Funds of Shandong University" under Grant no. 31370074614039. We would like to thank Prof. A. Abderrahmani (University of Lille 2) for providing the human serum sample.

References

1 J. Wang, *Chem. Rev.*, 2008, **108**, 814.
2 J. C. Pickup, F. Hussain, N. D. Evans, O. J. Rolinski and D. J. S. Birch, *Biosens. Bioelectron.*, 2005, **20**, 2555.
3 A. Heller and B. Feldman, *Chem. Rev.*, 2008, **108**, 2482.
4 M.-S. Steiner, A. Duerkop and O. S. Wolfbeis, *Chem. Soc. Rev.*, 2011, **40**, 4805.
5 Q. Wu, L. Wang, H. Yu, J. Wang and Z. Chen, *Chem. Rev.*, 2011, **111**, 7855.
6 K. E. Toghill and R. G. Compton, *Int. J. Electrochem. Sci.*, 2010, **5**, 1246.
7 G. Wang, X. He, L. Wang, A. Gu, Y. Huang, B. Fang, B. Geng and X. Zhang, *Microchim. Acta*, 2013, **180**, 161.
8 S. Park, H. Boo and T. D. Chung, *Anal. Chim. Acta*, 2006, **556**, 46.
9 J. M. Marioli and T. J. Kuwana, *Electrochim. Acta*, 1992, **37**, 1187.
10 M. Z. Luo and R. P. Baldwin, *J. Electroanal. Chem.*, 1995, **387**, 87.
11 C. Batchelor-McAuley, Y. Du, G. G. Wildgoose and R. G. Compton, *Sens. Actuators, B*, 2008, **135**, 230.
12 Z. Zhuang, X. Su, H. Yuan, Q. Sun, D. Xiao and M. M. F. Choi, *Analyst*, 2008, **133**, 126.
13 Y. Li, J. Fu, R. Chen, M. Huang, B. Gao, K. Huo, L. Wang and P. K. Chu, *Sens. Actuators, B*, 2014, **192**, 474.
14 Y. Zhang, L. Su, D. Manuzzi, H. Valdés Espinosa de los Monteros, W. Jia, D. Huo, C. Hou and Y. Lei, *Biosens. Bioelectron.*, 2012, **31**, 426.
15 C. Kong, L. Tang, X. Zhang, S. Sun, S. Yang, X. Song and Z. Yang, *J. Mater. Chem. A*, 2014, **2**, 7306.
16 K. R. Ratinac, W. Yang, J. J. Gooding, P. Thordarson and F. Braet, *Electroanalysis*, 2011, **23**, 803.

17 S. Wu, Q. He, C. Tan, Y. Wang and H. Zhang, *Small*, 2013, **9**, 1160.
18 M. Pumera, A. Ambrosi, A. Bonanni, E. L. K. Chng and H. L. Poh, *Trends Anal. Chem.*, 2010, **29**, 954.
19 T. Kuila, S. Bose, P. Khanra, A. K. Mishra, N. H. Kim and J. H. Lee, *Biosens. Bioelectron.*, 2011, **26**, 4637.
20 Y. Shao, J. Wang, H. Wu, J. Liu, I. A. Aksay and Y. Lin, *Electroanalysis*, 2010, **22**, 1027.
21 A. Ehsani, B. Jaleh and M. Nasrollahzadeh, *J. Power Sources*, 2014, **257**, 300.
22 P. He, W. Wang, L. Du, F. Dong, Y. Deng and T. Zhang, *Anal. Chim. Acta*, 2012, **739**, 25.
23 K. Zhang, *Appl. Surf. Sci.*, 2012, **258**, 7327.
24 Y. Yang, Z.-H. Lu, Y. Hu, Z. Zhang, W. Shi, X. Chen and T. Wang, *RSC Adv.*, 2014, **4**, 13749.
25 P. Fakhri, B. Jaleh and M. Nasrollahzadeh, *J. Mol. Catal. A: Chem.*, 2014, **383–384**, 17.
26 P. Mondal, A. Sinha, N. Salam, A. S. Roy, N. R. Jana and S. M. Islam, *RSC Adv.*, 2013, **3**, 5615.
27 Q. Chen, L. Zhang and G. Chen, *Anal. Chem.*, 2012, **84**, 171.
28 J. Luo, S. Jiang, H. Zhang, J. Jiang and X. Liu, *Anal. Chim. Acta*, 2012, **709**, 47.
29 L. Luo, L. Zhu and Z. Wang, *Bioelectrochemistry*, 2012, **88**, 156.
30 D. Jiang, Q. Liu, K. Wang, J. Qian, X. Dong, Z. Yang, X. Du and B. Qiu, *Biosens. Bioelectron.*, 2014, **54**, 273.
31 Z. Wang, J. Xia, X. Qiang, Y. Xia, G. Shi, F. Zhang, G. Han, L. Xia and J. Tang, *Int. J. Electrochem. Sci.*, 2013, **8**, 6941.
32 J. Luo, H. Zhang, S. Jiang, J. Jiang and X. Liu, *Microchim. Acta*, 2012, **177**, 485.
33 L. Xi, F. Wang, Z. Zhu, Z. Huang and Y. Zhu, *Talanta*, 2014, **119**, 440.
34 P. Subramanian, J. Niedziolka-Jonsson, A. Lesniewski, Q. Wang, M. Li, R. Boukherroub and S. Szunerits, *J. Mater. Chem. A*, 2014, **2**, 5525.
35 O. Fellahi, M. R. Das, Y. Coffinier, S. Szunerits, T. Hadjersi, M. Maamache and R. Boukherroub, *Nanoscale*, 2011, **3**, 4662.
36 Q. Wang, I. Kaminska, J. Niedziolka-Jonsson, M. Opallo, M. Li, R. Boukherroub and S. Szunerits, *Biosens. Bioelectron.*, 2013, **50**, 331–337.
37 M. Mazur, A. Barras, V. Kuncser, A. Galatanu, V. Zaitzev, K. V. Turcheniuk, P. Woisel, J. Lyskawa, W. Laure, A. Siriwardena, R. Boukherroub and S. Szunerits, *Nanoscale*, 2013, **5**, 2692.
38 S. J. An, Y. Zhu, S. H. Lee, M. D. Stoller, T. Emilsson, S. Park, A. Velamakanni, J. An and R. S. Ruoff, *J. Phys. Chem. Lett.*, 2010, **1**, 1259.
39 D. Janas and K. K. Koziol, *Nanoscale*, 2014, **6**, 3037.
40 A. Chavez-Valdez, M. S. P. Shaffer and A. R. Boccaccini, *J. Phys. Chem. B*, 2013, **117**, 1502.
41 M. H. Chakrabarti, C. T. J. Low, N. P. Brandon, V. Yufit, M. A. Hashim, M. F. Irfan, J. Akhtare, E. Ruiz-Trejo and M. A. Hussain, *Electrochim. Acta*, 2013, **107**, 425.
42 P. Subramanian, A. Lesniewski, I. Kaminska, A. Vlandas, A. Vasilescu, J. Niedziolka-Jonsson, E. Pichonat, H. Happy, R. Boukherroub and S. Szunerits, *Biosens. Bioelectron.*, 2013, **50**, 239.
43 P. Subramanian, F. Barka-Bouaifel, J. Bouckaert, N. Yamakawa, R. Boukherroub and S. Szunerits, *ACS Appl. Mater. Interfaces*, 2014, **6**, 5422.
44 C.-K. Wu, M. Yin, S. O'Brien and J. T. Koberstein, *Chem. Mater.*, 2006, **18**, 6054.
45 M. C. Biesinger, L. W. M. Lau, A. R. Gerson and R. S. C. Smart, *Appl. Surf. Sci.*, 2010, **257**, 887.
46 X. Zhou, H. Nie, Z. Yao, Y. Dong, Z. Yang and S. Huang, *Sens. Actuators, B*, 2012, **168**, 1.
47 H.-X. Wu, W.-M. Cao, Y. Li, G. Liu, Y. Wen, H.-F. Yang and S.-P. Yang, *Electrochim. Acta*, 2010, **55**, 3734.
48 X. Kang, Z. Mai, X. Zou, P. Cai and J. Mo, *Anal. Biochem.*, 2007, **363**, 143.
49 X. Zhang, G. Wang, W. Zhang, Y. Wei and B. Fang, *Biosens. Bioelectron.*, 2009, **24**, 3395.
50 L.-C. Jiang and W.-D. Zhang, *Biosens. Bioelectron.*, 2010, **25**, 1402.
51 F. Jiang, S. Wang, J. Lin, H. Jin, L. Zhang, S. Huang and J. Wang, *Electrochem. Commun.*, 2011, **13**, 363.
52 S. V. Prabhu and R. P. Baldwin, *Anal. Chem.*, 1989, **61**, 852.
53 M. Li, L. Liu, Y. Xiong, X. Liu, A. Nsabimana, X. Bo and L. Guo, *Sens. Actuators, B*, 2015, **207**, 614.